SEG Special Publications, no. 24, v. 2, pp. 297–310

Chapter 16

Fractionation of Sulfide Phases Controls the Chalcophile Metal Budget of Arc Magmas: Evidence from the Chilas Complex, Kohistan Arc, Pakistan

Ijaz Ahmad,[1,2,3,†] Jeremy P. Richards,[1,2,*] D. Graham Pearson,[3] Jingao Liu,[3,4] Sarah-Jane Barnes,[5] Pedro J. Jugo,[1] Muhammad T. Shah,[6] Matthew Leybourne,[7] and Oliver Jagoutz[8]

[1]*Mineral Exploration Research Centre, Harquail School of Earth Sciences, Laurentian University, 935 Ramsey Lake Road, Sudbury, Ontario, Canada P3E 2C6*

[2]*Department of Earth and Atmospheric Sciences, University of Alberta, Edmonton, Alberta, Canada T6G 2E3*

[3]*Abdul Wali Khan University Mardan, Mardan KP 23200, Pakistan*

[4]*Laboratory of Geological Processes and Mineral Resources, China University of Geosciences, Beijing 100083, China*

[5]*Université du Québec à Chicoutimi, Sciences de la Terre, Chicoutimi, Quebec, Canada G7H 2B1*

[6]*National Centre of Excellence in Geology, University of Peshawar, Peshawar KP 2500, Pakistan*

[7]*Queen's Facility for Isotope Research (QFIR), Department of Geological Sciences and Geological Engineering, Queen's University, Kingston, Ontario, Canada K7L 3N6*

[8]*Earth, Atmospheric and Planetary Sciences Department, Massachusetts Institute of Technology, 77 Massachusetts Avenue, Cambridge, Massachusetts 02139*

Abstract

Some arc magmas lead to the formation of porphyry deposits in the relatively shallow upper crust (<5 km). Porphyry deposits are major sources of Cu and an important Au source but lack significant amounts of platinum group elements (PGE). Sulfide phases control the behavior of chalcophile elements and affect the potential to form ore deposits either by remaining in the mantle residue or by fractionating from arc magmas at lower crustal levels, although in detail the role of sulfide saturation in the lower crust remains poorly understood. Lower crustal cumulate rocks from the 85 Ma Chilas Complex of the Kohistan arc, Pakistan, provide insight into processes that occur at depth in arcs. Here we provide Cu, Ni, Au, and PGE concentrations and Os isotope ratios of the Chilas Complex in order to constrain the extent of sulfide saturation in the lower crust and the effect of sulfide saturation on the metal budget of evolved melts that ascend to the upper crust. The Chilas rock suite contains less than 0.17 wt % sulfides and low PGE concentrations. In situ laser ablation-inductively coupled plasma-mass spectrometry (LA-ICP-MS) measurements of the sulfide inclusions in silicate minerals show enrichment in several chalcophile elements (up to 34 wt % Cu, 23 ppm Au, 245 ppm Pd, and 20 ppm Pt), whereas iridium group PGE (IPGE- Os, Ir, Ru) are mainly below detection limits. The metal content of the parental melt was modeled based on the elemental concentrations of the sulfides. The modeled parental arc magmas contain 70 to 140 ppm Cu, 0.2 to 1.5 ppb Au, and 1.2 to 8 ppb Pd, but low concentrations of IPGE, suggesting that IPGE were likely retained in the mantle source. Mass balance calculations show that segregation of a sulfide melt in the lower crust could further deplete the melt by more than 95% in Pd and Pt, 33 to 85% in Au, and 13 to 60% in Cu. Thus, magmas that ascend to the upper crust would contain very low concentrations of Au (< 0.2 ppb) and Pd (< 0.04 ppb), but they would retain sufficient concentration of Cu (~45–57 ppm) to form porphyry Cu deposits upon emplacement in the upper crust, as is commonly observed in arc settings.

Introduction

In contrast to other mantle-derived magmas such as midocean ridge basalt, magmas generated in arc settings during active subduction are generally sulfur and volatile-rich (900–2,500 ppm S; 2–6 wt % H_2O; 500–2,000 ppm Cl) and moderately oxidized (Δ_{FMQ} = 0.5–2; where Δ_{FMQ} is $\log f_{O_2}$ deviation from the fayalite-magnetite-quartz buffer), due to volatile release during slab dehydration and metasomatism of the mantle wedge (e.g., Ballhaus et al., 1990; De Hoog et al., 2003; Sharma et al., 2004; Wallace, 2005; Zimmer et al., 2010; Plank et al., 2013; Van Hoose et al., 2013). In arc magmas, sulfur is present in the melt as a combination of sulfide (S^{-2}) and sulfate (S^{+6}) species (Carroll and Rutherford, 1985; Jugo, 2009; Jugo et al., 2010; Evans and Tomkins, 2011). These melts may attain sulfide saturation in the lower crust due to cooling, crustal assimilation, and fractional crystallization (Mavrogenes and O'Neill, 1999; Lesher and Burnham, 2001; Robertson et al., 2015). When this occurs, chalcophile elements (Cu, Au, and platinum group elements, PGE: metals of economic

*Deceased June 7, 2019
†Corresponding author: e-mail, iahmad@laurentian.ca

Open Access (CC-BY-NC) publication of the Jeremy P. Richards memorial volume was generously supported by BHP Metals Exploration and the Laurentian University Mineral Exploration Research Centre (MERC) and Harquail School of Earth Sciences (HES).

Supplementary files are available online at www.segweb.org/SP24-VOL2-Appendices.
doi: 10.5382/SP.24.16; 14 p.

interest in arc settings) will partition into sulfide phases and precipitate in the lower crust, removing a significant fraction from the remaining melt (Richards, 2009, 2011; Lee et al., 2012; Thakurta et al., 2014; Holwell et al., 2019).

The extent to which sulfide phases are enriched in chalcophile elements depends on their partition coefficients ($D^{sulf/sil}$), their initial abundance in the melt C_i, and the mass ratio of silicate melt to sulfide melt interaction (R factor; Campbell and Naldrett, 1979). Relatively abundant chalcophile elements such as Cu (50–90 ppm in primitive arc magmas; Lee et al. 2012) with moderate partition coefficients ($(D_{Cu})^{sulf/sil} \approx 1{,}500$; Mungall and Brenan, 2014) will behave very differently compared to low-concentration PGE, such as Pt (~7 ppb; Becker et al., 2006), because of their very high partition coefficients (e.g. $(D_{Pt})^{sulf/sil} \approx 8.5 \times 10^5$; Mungall and Brenan, 2014). Under conditions of moderate silicate/sulfide melt ratio (R factor $\approx 10^2$–10^5; Richards, 2009) relatively small volumes of sulfide (~0.1 wt %; Hao et al., 2019) precipitating from the melt are predicted to host the bulk of the PGE due to their strong partitioning into sulfide phases (Richards, 2011). Segregation of these sulfide phases in the lower crust would strongly deplete the melt in PGE and to a moderate extent in Au, whereas Cu would be less affected due to its lower sulfide-melt partition coefficient (Richards, 2009; Du and Audétat, 2020). Therefore, such magmas could ascend and eventually form Cu-rich yet PGE-Au-depleted porphyry-style deposits (Richards, 2009, 2011).

An alternate view proposes that the mantle source of arc magmas is relatively reduced (i.e., not significantly different than MORB) with f_{O_2} in the range $-1 < \Delta_{FMQ} < 0$ (Lee et al., 2005, 2010; Mallmann and O'Neill, 2009; Tang et al., 2018) and would exsolve larger volumes of sulfide (~1%) in the lower crust (Lee et al. 2012). Retention of these sulfides in the lower crust would deplete the residual melt in PGE, Au, and also Cu (because of the larger volume of sulfides that would form). A consequence of such a model is that the formation of porphyry Cu deposits would requires a second step of remobilization of these sulfides during arc magmatism (Jenner et al., 2010; Lee et al., 2012; Chiaradia, 2014; Jenner, 2017; Chen et al., 2020; Lee and Tang, 2020). The key to assessing the validity and feasibility of these contrasting models is to constrain the chalcophile metal content in whole rocks and sulfides from the rare samples that represent lower crust in arc settings. Here, we provide Cu, Ni, Au, and PGE concentration data for cumulate rocks and their sulfides from one of the best exposed lower crustal arc sections in the world: the Chilas Complex of the Cretaceous-Paleogene Kohistan paleo-arc, northern Pakistan. The rocks contain a relatively small fraction of sulfides (≤0.17 wt %), but the sulfides have relatively high concentrations of Cu (≤34 wt %), Au (≤23 ppm), Pd (≤245 ppm), and Pt (≤20 ppm). These findings are consistent with a model involving minor, but pervasive early sulfide saturation in parental arc melts, leading to PGE-Au-depleted but relatively Cu-undepleted fractionated magmas that have the potential to form typical subduction-related porphyry Cu deposits.

Kohistan Arc

The Kohistan island arc developed during the Cretaceous-Paleogene by northward subduction of the Indian plate in equatorial regions of Neo-Tethys Ocean and was accreted between the Eurasian (Karakoram) and Indian plates (Tahirkheli and Jan, 1979; Khan et al., 2009; Petterson, 2010; Burg, 2011). The Kohistan island arc is estimated to have collided with Eurasia between 102 and 85 Ma, followed by the collision of India with the combined Kohistan-Eurasia block at about 50 Ma (Patriat and Achache, 1984; Petterson and Windley, 1985; Khan et al., 1993; Treloar et al., 1996; Petterson, 2019). However, Bouilhol et al. (2013) and Jagoutz et al. (2015) proposed a different sequence of events—the India-Kohistan island arc collision occurred at ~50 Ma, followed by a final collision with Eurasia at ~44 Ma.

The Southern Plutonic Complex and the Chilas Complex (Fig. 1A) are two distinct lower crustal sections of the Kohistan arc (Jagoutz et al., 2009). The Southern Plutonic Complex is structurally deeper and relatively older, having formed before ~95 Ma (Burg et al., 2006). The Chilas Complex is relatively younger (85–81 Ma; Schaltegger et al., 2002), undeformed, with no pervasive surficial alteration, and exposed over a larger area (~300 × 40 km; Khan et al., 1989).

Mafic rocks comprise the bulk of the Chilas Complex and consist of gabbro, norite, and diorite (gabbronorite association; Khan et al., 1989). These cumulates are largely homogeneous but locally layered (Jagoutz et al., 2006; Fig. 1B). The complex also contains a few ultramafic bodies (ultramafic-mafic association; Khan et al., 1993; Jagoutz et al., 2006) and late feldspar-hornblende-pyroxene pegmatite lenses (Fig. 1C). Although the contact relationship of ultramafic bodies and the gabbronorite rocks are complex, the rocks are interpreted to be cogenetic based on geochemistry (Khan et al., 1989; Jagoutz et al., 2006).

The northern section of the Kohistan arc consists of metasedimentary rocks of the Jaglot Group (~125–99 Ma), overlain by the Chalt and Shamran Volcanic groups (~99–32 Ma), which consists of pillowed and massive boninite, basalt, and andesite flows (Petterson and Treloar, 2004). The Yasin Group sedimentary rocks (~125–99 Ma) rest conformably on top of the Chalt Volcanic Group and contain sandstone, siltstone, and minor carbonates (Robertson and Collins, 2002). The mid to upper plutonic crust of the Kohistan island arc comprises intermediate-to-felsic rocks of the Kohistan batholith, part of the Trans-Himalayan batholith, that intruded these stratiform sequences mainly between 120 to 30 Ma (Fig. 1A; Jagoutz et al., 2009).

Samples and Methods

Twenty-six samples of gabbro and four dunite samples were selected from a larger suite of collected samples (n = 79), from three traverses of the Kohistan island arc (Fig. 1A). Whole-rock compositions were determined by Activation Laboratories (Ancaster, Ontario). Major elements were determined using inductively coupled plasma-atomic emission spectrometry (ICP-AES). Trace element concentrations were determined using ICP-mass spectrometry (ICP-MS) and instrumental neutron activation analysis (INAA; Actlabs analysis code 4E-Research + ICPMS). Fire assay ICP-MS was used for Au (Actlabs analysis code 1C-Research). The reproducibility of standard reference material is summarized in Appendix Table A1. Precise PGE analyses at lower detection limits (~0.4–0.6 ppt) and Os isotope ratios in whole-rock sam-

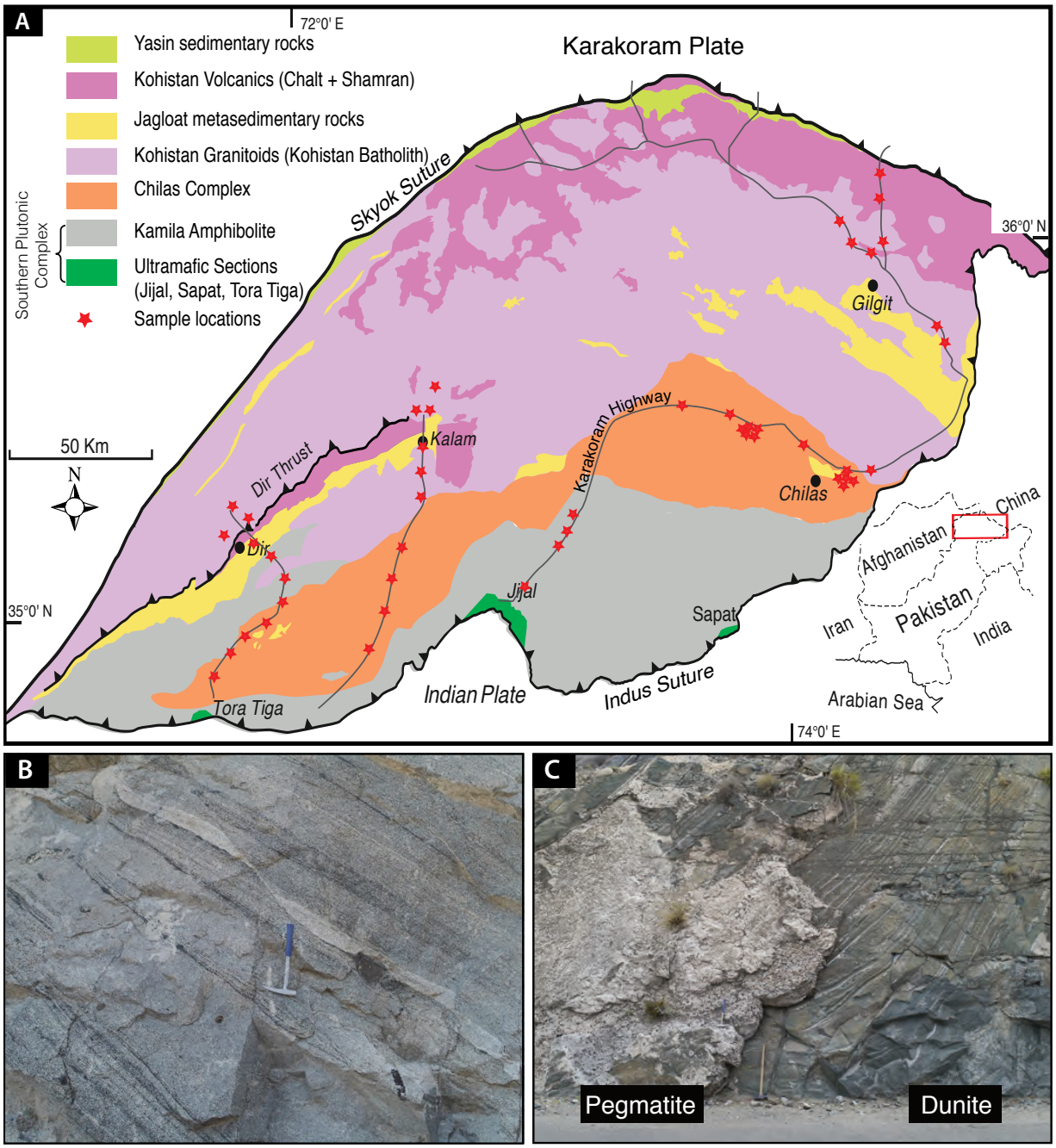

Fig. 1. A. Simplified geologic map of the Kohistan paleoarc, Pakistan (after Jagoutz et al., 2006) B. Layered gabbronorite of the Chilas Complex. C. Layered dunite of the Chilas Complex with crosscutting pegmatite.

ples were determined by isotope dilution, using the method of Pearson and Woodland (2000) and Liu and Pearson (2014), at the Arctic Resources Laboratory of the University of Alberta. Measured standard and blank composition are reported in Table A2.

Sulfide inclusions consist of pyrrhotite-pentlandite-chalcopyrite (Po-Pn-Ccp; Fig. 2A-C). Unexposed sulfide inclusions (Fig. 2D-E) hosted by silicate minerals (mainly olivine, pyroxene and amphibole) were selected to determine the chalcophile element compositions of the entire inclusions, using 100-µm-thick polished sections. The concentration of S, Fe, Cu, Ni, Co, PGE, and Au were determined by LA-ICP-MS at the LabMaTer, University of Quebec at Chicoutimi (UQAC), using an Excimer 193-nm RESOlution M-50 laser ablation system (Australian Scientific Instrument) equipped with a double volume cell S-155 (Laurin Technic), coupled with an Agilent 7900 mass spectrometer. LA-ICP-MS operating parameters were as follows: a laser frequency of 15 to 30 Hz, peak dwell times of 20 ms for PGE and Au, and 5 ms for all other elements, and a fluence of 3 J/cm^2. Spot analyses were used, with laser beam sizes ranging from 33 to 55 µm in diameter, depending on the size of the sulfide inclusion. To ensure

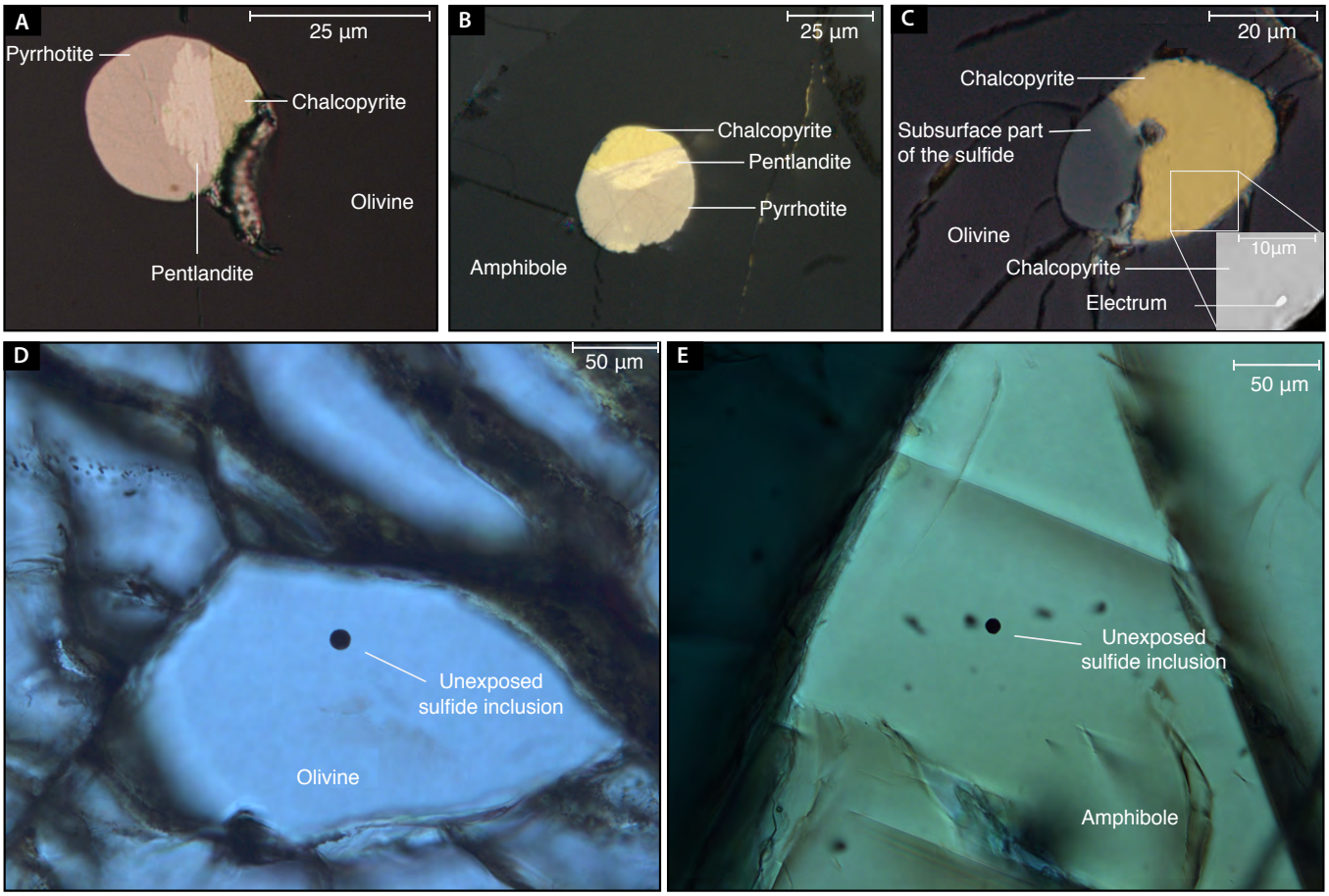

Fig. 2. A.-B. Representative example of sulfide inclusions in olivine from dunite (sample K11) and amphibole from gabbro (sample K11b). C. Example of chalcopyrite inclusion hosting electrum inclusion (inset SEM image) from the Thurley dunite (sample K6). D.-E. Photomicrograph showing unexposed sulfide inclusions in olivine from a dunite sample (K11) and amphibole from a gabbro sample (K3).

complete ablation of the entire sulfide droplets, the beam size was made slightly larger than the inclusion, ablating parts of the host. The gas blank was measured for 20 s before switching on the laser and drilling through the silicate host, through the sulfide inclusion, and back into the silicate host, generally producing a sulfide signal of 30- to 60-s duration (Fig. 3). The ablated material was carried into the ICP-MS by an Ar-He-N_2 gas mix at a rate of 0.8 to 1 L/min for Ar, 350 mL/min He, and 2mL/min N_2.

The masses monitored correspond to the following isotopes: ^{24}Mg, ^{27}Al, ^{28}Si, ^{29}Si, ^{33}S, ^{34}S, ^{43}Ca, ^{44}Ca, ^{47}Ti, ^{49}Ti, ^{51}V, ^{53}Cr, ^{55}Mn, ^{57}Fe, ^{59}Co, ^{60}Ni, ^{61}Ni, ^{63}Cu, ^{65}Cu, ^{66}Zn, ^{68}Zn ^{75}As, ^{77}Se, ^{82}Se, ^{95}Mo, ^{99}Ru, ^{101}Ru, ^{103}Rh, ^{105}Pd, ^{106}Pd, ^{108}Pd, ^{107}Ag, ^{109}Ag, ^{111}Cd, ^{115}In, ^{118}Sn, ^{121}Sb, ^{125}Te, ^{185}Re, ^{189}Os, ^{190}Os, ^{193}Ir, ^{194}Pt, ^{195}Pt, ^{197}Au, ^{202}Hg, ^{208}Pb, ^{209}Bi. Po727, a synthetic FeS, supplied by Memorial University of Newfoundland, doped with ~40 ppm PGE and Au was used to calibrate Fe and S. UQAC-FeS1, a synthetic sulfide doped with Ni, Cu and 40 to 100 ppm of most chalcophile elements (Mansur et al., 2020; Table A3) was used calibrated for Co, Ni, Cu, PGE, and Au. GSE-1g, a natural basaltic glass supplied by the U.S. Geological Survey, doped with many trace elements at 300 to 500 ppm, was used to monitor the silicate component of the signal, using the Georem preferred values (Jochum et al., 2005). JB-MSS5, a synthetic FeS, supplied by James Brenan, containing 50 to 70 ppm of most chalcophile elements (Patten et al., 2013), was used as a secondary standard to monitor the results (Table A3).

Polyatomic interferences of ^{63}Cu^{40}Ar on ^{103}Rh and ^{65}Cu^{40}Ar on ^{105}Pd were corrected using a Cu-blank (PGE-free Cu wire), 1% Cu produced ~0.05 ppm Rh interference. Direct interference of ^{106}Cd on ^{106}Pd was corrected by monitoring ^{111}Cd. Interference of ^{61}Ni^{40}Ar on ^{101}Ru was corrected using an NiS sulfide with no detectable Ru. One percent Ni produced ~0.007 ppm Ru interference and was not a significant part of the Ru signal.

Data reduction of the ablated sulfide inclusions, including separation of the sulfide signal from the host, was done following the method of Chang and Audétat (2018). The method uses two external standards for quantification in two steps. In the first step, the Fe/S ratio of the sulfide inclusion is quantified based on the known Fe/S ratio of the Po727 standard. In the second step, all other elements are quantified using Fe as internal standard and UQAC-FeS1 as an external standard. The data is then normalized to 100 wt % using the sum of S, Fe, Ni, Co, and Cu. The ablation interval representing sulfide was carefully selected based on the S signal in sulfide inclusions (Fig. 3). The signal contribution from the host was

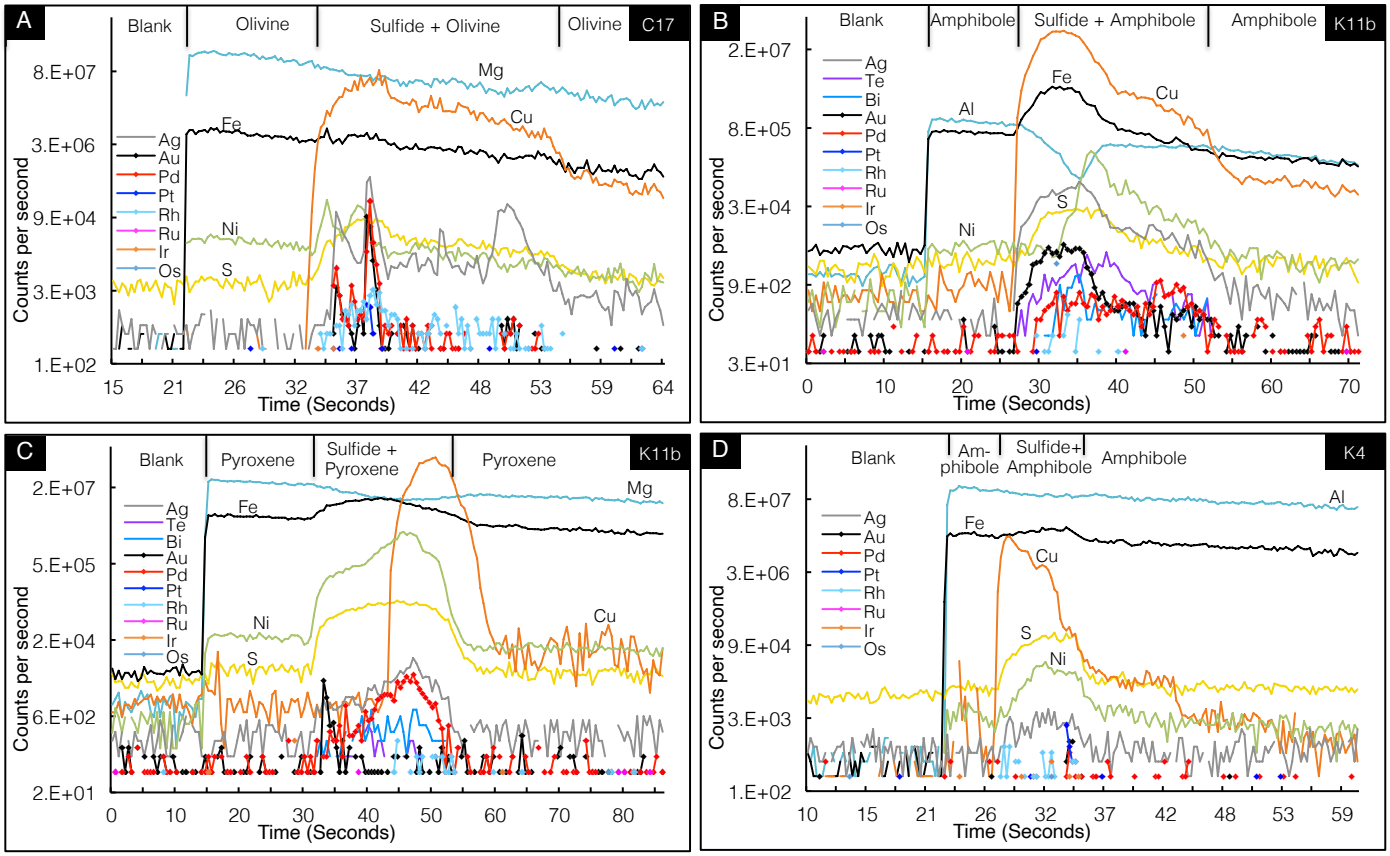

Fig. 3. Time-resolved spectra of sulfide inclusions. A. Cu-rich inclusions in olivine. B. Cu-rich inclusions in amphibole. C. MSS-type inclusions in pyroxene. D. MSS-type inclusions in amphibole. The sudden increase in the Cu count rates (panels A, B, and D) or Ni count rate (panel C) indicates the start of sulfide ablation. Changes in Ni and Cu counts indicate changes through different sulfides in the inclusions (as shown in Fig. 2A-B). The uneven distribution of PGE and Au indicates they are hosted as small inclusions (nanometer-scale) in the sulfides.

subtracted based on the Si signal. Standard JB-MSS5 was run as unknown every 10 analyses, and the calculated values for each element are within the uncertainty of their reported concentration (Table A3), which validates the method's accuracy. The relative uncertainty of our data is <3 to 8%, which is within the reported uncertainties of the method (≤5–10%; Zhang and Audétat, 2017; Chang and Audétat, 2018), suggesting that our quantification is accurate.

Results

Sulfide inclusions

Less than 25% of the samples studied from the Chilas Complex contain sulfides. Where present, the sulfide modal abundance is very low (<0.1 vol %). Sulfides typically occur as globular or subhedral micrometer-scale inclusions in silicate minerals (mainly olivine, pyroxene, and amphibole) and consist mainly of pyrrhotite with minor pentlandite and chalcopyrite (Fig. 2A-C). Because of their round section and mineral association, these inclusions are interpreted to represent sulfide melt droplets trapped in the cumulate silicate minerals, which then underwent crystallization and exsolution during cooling to form the discrete sulfide mineral phases observed. At the Thurly body (Khan et al., 1989), macroscopically visible sulfides (~2 vol %) occur interstitially between olivine crystals in a small zone (1–2 m in length and less than a meter in thickness) within a dunite body. An electrum inclusion was observed in chalcopyrite from this sample (Fig. 2C).

Whole-rock Os isotope ratios and chalcophile element compositions

The initial Os isotope ratios $(^{187}Os/^{188}Os)_i$ of 11 gabbro samples from the Chilas Complex range from 0.129 to 0.295, with two samples showing significantly higher values of 0.958 and 1.470. The four dunite samples yielded low $(^{187}Os/^{188}Os)_i$ ratios of 0.128 to 0.165 (Table 1). These values are within the range (0.127–3.15) of mantle-derived magmas (e.g., Gannoun et. al., 2016), with the elevated values likely indicating interaction with crust.

Platinum group element concentrations in the Chilas Complex gabbros (Fig. 4A; Table 1) are generally low relative to mantle with significant PPGE to IPGE fractionation (Ir ≤0.07 ppb, Os ≤0.03 ppb, Pt = 0.23–3.67 ppb, Pd = 0.07–7.67 ppb, Pt/Os = 22–224). The dunites mostly contain higher concentrations of PGE than gabbros and slightly less fractionated patterns (Ir = 0.31–1.05 ppb, Os = 0.19–0.89 ppb; Pt = 4.37–29.6 ppb, Pd = 3.3–22.4 ppb, Pt/Os = 23–104). Copper content varies from 11 to 44 ppm in the dunites and 7 to 119 ppm in gabbros, and mantle normalized Cu patterns (Fig. 4A) mostly show enrichment relative to PGE and Au. Gold in

Table 1. Location, Lithology, Whole-Rock Chalcophile Element Concentrations and Re-Os Isotope Ratios of the Chilas Complex Gabbros and Dunites (sample K6 is from a mineralized zone that extends for less than 2 m laterally and less than a meter vertically; see text for details)

Sample no.	C5	K11	C17	K6	K11B	K20	K2	K4	K7	D10	D11	D13	S4	S10
Projection	WGS 84, 43N	WGS 84, 43N	WGS 84, 43N	WGS 84, 43N	WGS 84, 43N	WGS 84, 43N	WGS 84, 43N	WGS 84, 43N	WGS 84, 43N	WGS 84, 42N	WGS 84, 42N	WGS 84, 42N	WGS 84, 43N	WGS 84, 43N
UTM (E)	401733	0422085	402901	0401746	0422085	0388857	0401279	0401242	0402851	773357	768339	761171	282929	271376
UTM (N)	3927130	3918742	3926216	3927174	3918742	3930850	3927377	3927381	3927117	3865743	3861551	3859445	3911562	3884496
TAS lithology	Dunite	Dunite	Dunite	Dunite	Subalkalic gabbro	Subalkalic gabbro	Subalkalic gabbro	Subalkalic gabbro	Gabbroic diorite	Gabbroic diorite	Gabbroic diorite	Gabbroic diorite	Gabbroic diorite	Gabbroic diorite
Ni (ppm)	1570	1170	1610	2010	575	94	92	34	43	67	25	59	54	62
Co (ppm)	197	185	177	106	83.9	160	37.5	24.1	31.9	32.5	26.5	31.9	28.9	35.3
Os (ppb)	0.19	0.28	0.89	5.3	0.02	0.02	0.03	0.01	0.01	0.01	0.01	0.01	0.01	0.02
Ir (ppb)	0.31	0.69	1.05	10.2	0.03	0.07	0.04	0.003	0.001	0.03	0.01	0.02	0.02	0.04
Pt (ppb)	4.37	29.63	25.33	533.0	3.67	1.01	3.35	0.33	2.14	2.20	0.23	1.44	1.07	2.79
Pd (ppb)	3.30	22.40	7.69	747.0	7.67	1.19	4.23	0.07	2.75	1.63	0.17	0.98	1.54	3.32
Re (ppb)	0.04	0.30	0.07	1.2	0.24	0.38	1.47	0.03	0.29	0.05	0.09	0.04	0.17	0.15
Au (ppb)	1	<LOD	<LOD	310.0	4	<LOD	2	<LOD	2	<LOD	<LOD	2	<LOD	<LOD
Cu (ppm)	11	44	13	4500	119	55	33	42	40	12	43	45	7	81
Pt/Os	23.4	104.7	28.4	100.9	224.2	62.7	129.7	22.1	209.5	184.8	22.5	139.8	152.3	141.8
$^{187}Re/^{188}Os$	1.1	5.1	0.4	1.1	76.5	126.3	335.7	11.4	159.8	20.7	44.3	20.2	119.3	37.1
$^{187}Os/^{188}Os$	0.185	0.134	0.165	0.146	0.329	0.302	1.417	1.486	0.357	0.253	0.363	0.251	0.276	0.195
$(^{187}Os/^{188}Os)_i$	0.183	0.128	0.165	0.145	0.225	0.129	0.958	1.470	0.139	0.222	0.295	0.220	0.083	0.141

Notes: Ni and Cu are analyzed by TD-ICP, Co by INAA, Au by fire assay ICP-MS, and PGE by isotope dilution; <LOD is below the detection limit (LOD for Au is 1 ppb and ranges from 0.4–0.6 ppt for PGE); initial Os isotope ratios ($^{187}Os/^{188}Os)i$ were calculated based on 85 Ma age for the Chilas Complex (Schaltegger et al., 2002)

both the rock types is less than 4 ppb, slightly more enriched than Pt and Pd, but more depleted than Cu. The sulfide-rich dunite sample (K6) from the Thurly body is anomalous, compared to the rest of the samples analyzed, and is enriched in Cu (4,500 ppm), Ni (2,010 ppm), Pt (533 ppb), Pd (747 ppb), and Au (310 ppb).

Major and trace element abundances in sulfide inclusions

Magmatic sulfide inclusions exsolved several mineral phases upon cooling, and analyses of exposed inclusions would not be representative. Therefore, to constrain their composition during entrapment, we report the bulk content of unexposed inclusions (contained in host minerals). Major and trace element data are presented in Table 2 and Figure 4B-C. Various populations of inclusions can be distinguished using the Fe-S-Cu phase diagram at 1,000ºC (Fig. 4B) as a frame of reference. Data from several analyses plot within or near the monosulfide solid solution field (MSS). Few inclusions plot within the Cu-rich sulfide liquid field (SL), and some in the region show the tie lines between the MSS and SL fields. The samples near the SL field (e.g., cluster of three K3 and one K11 samples) are consistent with the composition of a Cu-rich sulfide melt in equilibrium with MSS; by contrast, the cluster near the center of the diagram (cluster of K11b and a single C17 sample) is consistent with intermediate solid solution (ISS) that is expected to form at lower temperatures (T <900°C) from a fractionated Cu-rich sulfide melt.

As shown in Table 2, Cu-rich inclusions (with Cu ranging from 9.3–31.6 ± 2.7 wt %) have higher concentrations of elements that are more compatible with sulfide liquid than MSS (Liu and Brenan, 2015), such as Au (~0.07–12 ± 10 ppm), Pd (~6.3 ± 3–62.3 ± 100 ppm), Pt (~0.5–4.6 ± 8 ppm), Ag (~7.9–223 ppm), and Ni (~1.2 ± 0.6–15.3 wt %). In contrast, MSS-type inclusions show relatively lower concentration in these elements (Cu from ~2.3 ± 0.6–4.7 ± 2 wt %; Au <0.2 ppm; Pd from <0.1–4.4 ± 4 ppm; Pt <0.3 ppm; Ag from 2.3 ± 2.3–7.7 ± 2 ppm, and Ni from 0.4 ± 0.09–7.1 ± 2 wt % (Table 2). The osmium and Ru contents of all the inclusions were below detection limits; Ir, Rh, and Re are less than a ppm, Mo and Cd are in tens of ppm range, Zn and Se are in ten to hundreds of ppm range, Co in thousands of ppm range, and Pb is less than122 ppm (Table 2). Spikes in Au, Pd, and Pt count rates within the sulfide domain in time-resolved spectra (Fig. 3), and petrographic observation of electrum in chalcopyrite (Fig. 2C) indicate that these elements exist as submicrometer inclusions and not in solid solution. Although these features can cause nugget effects and there is some intrasample heterogeneity, we assume that by ablating entire sulfide blebs and averaging several inclusions, the results are reasonably representative of the sulfide phases prior to exsolution.

Discussion

Petrogenesis of the Chilas Complex magmas

Several workers have proposed a suprasubduction (mantle wedge) source for the Chilas magmas based on whole-rock geochemistry, mineralogy, and Nd-Sr-Hf isotope systematics (e.g., Mikoshiba et al., 1999; Schaltegger et al., 2002; Jagoutz et al., 2006). The initial Os isotope ratios for the Chilas cumu-

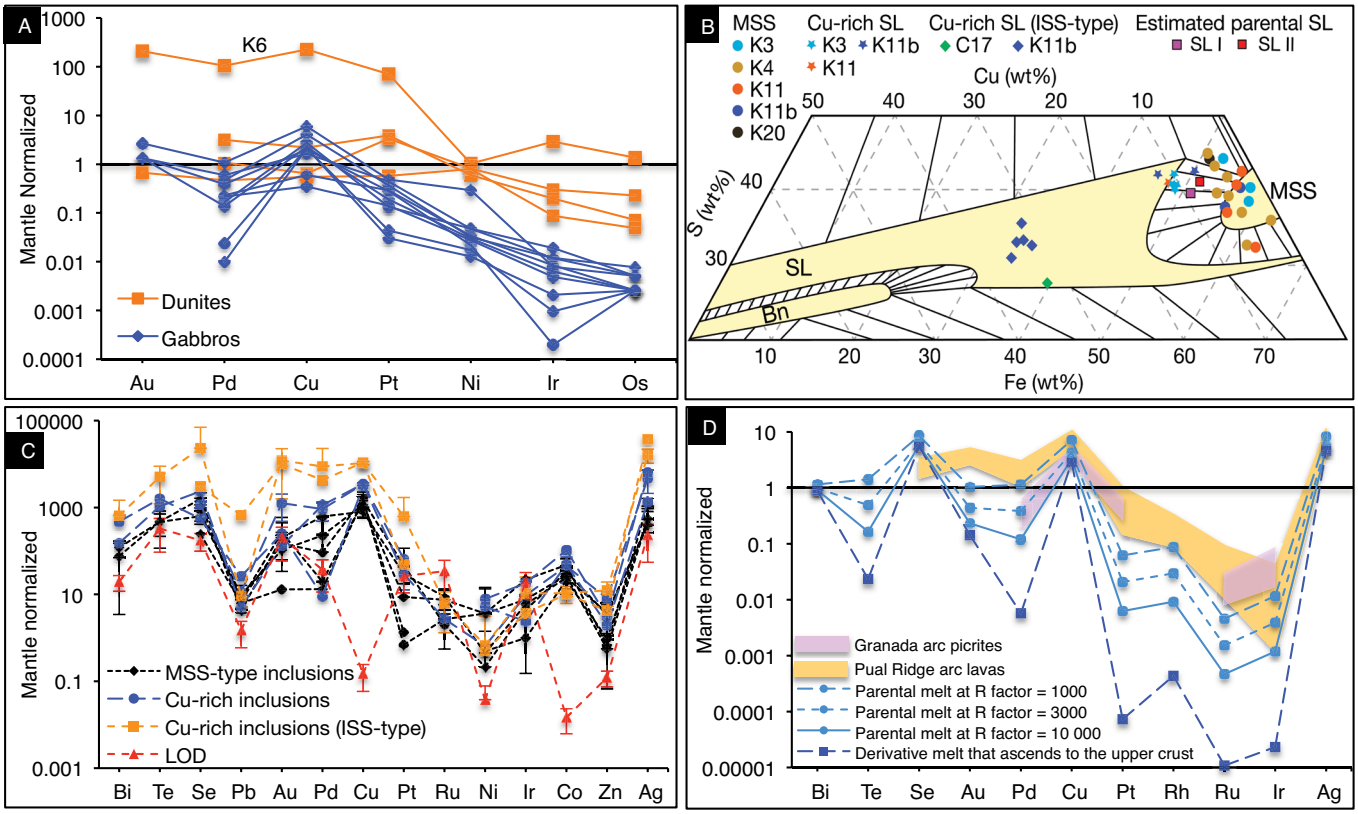

Fig. 4. A. Whole-rock content of selected chalcophile elements of gabbros and dunites from the Chilas Complex, normalized to primitive upper mantle (PUM). One dunite sample (K6) has anomalously high values compared to the other samples and contains visible sulfides in hand specimen. B. Composition of sulfide inclusions; for reference a portion of the Fe-S-Cu phase diagram at 1,000ºC is shown(Kullerud et al., 1969). The symbols labeled SL I and SL II are estimates of the primary sulfide melt composition (see text for detail). C. Mantle-normalized content of selected chalcophile elements in sulfide inclusions, showing enrichment in PGE, Au, and Cu. The Pt, Pd, and Au contents are highest in inclusions matching the Cu-rich sulfide liquid (ISS-type) composition. D. Calculated parental and derivative magma compositions for the Chilas Complex (PUM-normalized). According to calculations, the parental magmas were depleted in IPGE relative to PUM but contained Cu, Au, and Pd in concentrations similar or slightly above mantle values, and slightly depleted Pt concentrations. The obtained values are consistent with values from natural examples in other localities (Granada arc picrites; Pual Ridge arc lavas). Calculated derivative magmas are depleted in PGE and Au by incorporation of cumulate sulfides but to different extents (e.g., Ru and Ir are more strongly depleted than Pd or Au). However, Cu is not significantly affected. Mantle normalization values are from Palme and O'Neill (2014), Grenada data from Woodland et al. (2002), and Pual Ridge arc data from Park et al. (2013). Bn = bornite field, ISS = intermediate solid solution, MSS = monosulfide solid solution, SL = sulfide liquid.

lates, especially the dunites with higher Os contents, that are less susceptible to the effects of crustal contamination, mostly overlap or are slightly more radiogenic than the range of Os isotope compositions shown by PGE alloys derived from suprasubduction zone ophiolites ($^{187}Os/^{188}Os$ = 0.119–0.129); the compositions reflect a mix of depleted mantle and mantle slightly enriched by subduction zone processes (Pearson et al., 2007). Therefore, we interpret the Chilas rocks to have derived from partial melting of a subduction-modified mantle wedge. However, two of our gabbro samples have significantly higher values ($^{187}Os/^{188}Os$ = 0.96, 1.47), likely reflecting crustal assimilation of the Jagloat Group metasedimentary rocks, since xenoliths of these rocks are found within the complex (Fig. 1A; Mikoshiba et al., 1999).

Origin of the sulfide inclusions

Magmas emplaced in the lower crust of arc settings are typically assumed to be sulfide undersaturated due to the increasing S solubility in silicate melt with decreasing pressure (Mavrogenes and O'Neill, 1999). Thus, assimilation of S-rich sediments is commonly proposed as the mechanism required to induce sulfide saturation (Grinenko, 1985; Lesher and Burnham, 2001; Ripley and Li, 2003; Keays and Lightfoot, 2010; Fiorentini et al., 2012; Robertson et al., 2015). If sulfide saturation is reached, the initial sulfide melt starts to crystallize MSS when the system cools below ~1,120°C. Extraction of MSS results in Cu-rich residual melts, which subsequently crystallize ISS on further cooling below ~950°C (e.g., Cabri, 1973; Holwell and McDonald, 2010; Kosyakov and Sinyakova, 2012; Mansur et al., 2020). Sulfides of the Chilas Complex are consistent with a similar crystallization sequence. Entirely unexposed sulfide inclusions in the Chilas Complex show that the sulfide melt fractionated to MSS and Cu-rich sulfide liquid (Fig. 4B; Table 2). Three samples (K3, K11, K11b) contain both MSS and Cu-rich inclusions, with a set of highly fractioned ISS-type inclusions in sample K11b (Table 2). Sul-

Table 2. Major and Trace Element Compositions of Sulfide Inclusions

Inclusions	K11-1	K11-2	K11-3	K11-4	K11-5	C17	K11b-1	K11b-2	K11b-3
Rock type	Dunite	Dunite	Dunite	Dunite	Dunite	Dunite	Subalkalic gabbro	Subalkalic gabbro	Subalkalic gabbro
Host mineral	Olivine	Olivine	Olivine	Olivine	Olivine	Olivine	Pyroxene	Pyroxene	Amphibole
Inclusion-type	MSS	MSS	MSS	Cu-rich SL	MSS	Cu-rich SL (ISS-type)	MSS	Cu-rich SL	MSS
S (wt %)	39.0	39.7	29.5	34.6	34.1	27.0	38.7	37.8	35.1
Fe (wt %)	53.5	51.5	56.5	40	51.95	39.26	45.3	41	51.85
Co (wt %)	0.3	0.4	0.7	1.1	0.6	0.1	0.4	0.5	0.4
Ni (wt %)	4.4	6.6	9.5	15.4	8.0	1	8.9	10.2	7.4
Cu (wt %)	2.9	1.4	4.2	9.3	5.4	32.7	6.4	10.5	5.3
Zn (ppm)	12.2	–8.2	48.4	163.6	74.8	222.5	15.9	105.3	64.6
As (ppm)	<2.6	<4.3	3.46	<4.6	<5.1	<3.2	1.4	2.04	<4.2
Se (ppm)	23.1	53.8	55.8	42.3	58.0	227.1	168.6	178.4	110.3
Mo (ppm)	<3.4	<3.8	<2.8	5.8	<3.9	<0.3	1.9	3.3	<5.6
Ru (ppm)	<0.2	<0.3	<0.2	<0.3	<0.3	<0.1	<0.04	<0.1	<0.2
Rh (ppm)	<0.03	<0.05	<0.04	<0.04	0.09	<0.45	<0.005	<0.03	<0.04
Pd (ppm)	<0.3	<0.4	<0.2	<0.6	4.6	30.5	1.8	8	<0.6
Ag (ppm)	8.9	4.9	7.6	38.6	9.5	223.2	2.4	7.9	6.8
Cd (ppm)	<1.5	<2.1	0.8	<2.9	3.7	18.4	<0.4	<0.9	<0.7
In (ppm)	0.4	<0.2	<0.3	<0.3	0.1	1.3	<0.06	0.1	<0.4
Sn (ppm)	0.5	<0.6	<0.6	<1.08	<0.5	n.a.	<0.1	<0.5	<0.9
Sb (ppm)	<0.3	<0.5	<0.5	0.4	<0.3	n.a.	<0.0	<0.2	0.3
Te (ppm)	<2.5	7.4	3.8	14.5	<3.3	n.a.	1.9	9.6	7.9
Re (ppm)	0.5	<0.1	0.2	0.1	0.4	<0.2	0.3	0.1	0.2
Os (ppm)	<0.2	<0.2	<0.2	<0.3	<0.3	<0.1	<0.04	<0.1	<0.4
Ir (ppm)	<0.05	<0.09	<0.08	<0.1	<0.1	<0.03	<0.01	<0.05	<0.1
Pt (ppm)	<0.1	<0.2	<0.2	<0.2	<0.3	0.36	<0.03	0.5	<0.3
Au (ppm)	<0.5	<0.2	<0.3	<0.4	<0.5	10	0.2	<0.3	<0.3
Hg (ppm)	<3.8	<5.2	<3.7	<5.6	<10.6	n.a.	<2.09	<2.3	<5.2
Pb (ppm)	1.5	1.4	2.2	4.8	2.1	122.6	0.3	0.9	2.5
Bi (ppm)	0.5	0.4	0.4	1.4	0.1	n.a.	0.1	0.5	0.5
Mg number	0.845	0.846	0.848	0.841	0.842	0.846			

Inclusions	K11b-4	K11b-5	K11b-6	K11b-7	K11b-8	K11b-9	K11b-10	K3-1
Rock type	Subalkalic gabbro	Subalkalic gabbro	Subalkalic gabbro	Subalkalic gabbro	Subalkalic gabbro	Subalkalic gabbro	Subalkalic gabbro	Subalkalic gabbro
Host mineral	Pyroxene	Pyroxene	Amphibole	Amphibole	Amphibole	Plagioclase	Amphibole	Amphibole
Inclusion-type	MSS	Cu-rich SL (ISS-type)	Cu-rich SL (ISS-type)	Cu-rich SL (ISS-type)	Cu-rich SL (ISS-type)	Cu-rich SL (ISS-type)	Cu-rich SL (ISS-type)	Cu-rich SL
S (wt %)	38.6	32.7	30.5	18.8	33.4	35.9	32.9	40.4
Fe (wt %)	53.75	32.55	33.1	50.25	33.5	31.5	34.6	48
Co (wt %)	0.1	0.2	0.1	0.1	0.0	0.1	0.2	0.1
Ni (wt %)	5.1	1.7	1.7	2.0	1.0	0.9	0.7	0.5
Cu (wt %)	2.5	33.0	34.7	28.9	32.1	31.3	31.5	11.0
Zn (ppm)	8.7	687.7	342.4	593.4	456.9	575.0	1354.0	326.5
As (ppm)	<5.3	<1.8	<1.6	<2.6	<2.4	<4.6	<3.3	<8.6
Se (ppm)	77.5	303.9	178.8	844.7	288.0	69.0	8899.1	79.1
Mo (ppm)	<4.9	2.1	<1.1	<1.6	<2.4	<0.2	<0.2	64.6
Ru (ppm)	<0.3	<0.1	<0.1	<0.1	<0.2	<0.1	<0.1	<0.3
Rh (ppm)	<0.06	<0.01	<0.01	0.04	<0.04	<0.03	0.2	<0.06
Pd (ppm)	<0.6	0.3	10.4	2.7	1.6	110.3	245.06	7.4
Ag (ppm)	<1.3	76.3	156.8	111.7	66.8	103.2	68.5	21.4
Cd (ppm)	<1.9	7.03	8.2	16.2	13.9	3.01	7.4	<2.5
In (ppm)	<0.4	1.1	0.9	1.9	0.6	1.2	1.6	<0.2
Sn (ppm)	<0.9	<0.2	0.8	0.8	<0.5	n.a.	n.a.	n.a.
Sb (ppm)	<0.6	<0.2	<0.1	<0.3	<0.2	n.a.	n.a.	n.a.
Te (ppm)	2.9	38.9	40.0	98.3	10	n.a.	n.a.	n.a.
Re (ppm)	<0.1	<0.06	0.09	<0.08	<0.1	<0.06	<0.05	0.8
Os (ppm)	<0.3	<0.1	<0.1	0.5	<0.2	<0.08	<0.1	<0.3
Ir (ppm)	<0.1	<0.03	<0.03	<0.05	<0.08	<0.03	0.1	<0.1
Pt (ppm)	<0.2	<0.09	1.1	<0.1	<0.2	4.7	19.4	<0.1
Au (ppm)	<0.2	1.6	18.1	6.5	0.6	22.5	22.7	2.2
Hg (ppm)	<4.6	<1.8	2.5	5.6	3.7	n.a.	n.a.	n.a.
Pb (ppm)	-0.7	1.5	0.6	2.1	1.5	2.8	1.5	1.9
Bi (ppm)	-0.1	0.2	5.5	0.6	1.5	n.a.	n.a.	n.a.
Mg number								

Table 2. (Cont.)

Inclusions	K3-2	K3-3	K3-4	K3-5	K3-6	K3-7	K4-1	K4-2
Rock type	Subalkalic gabbro	Subalkalic gabbro	Subalkalic gabbro	Subalkalic gabbro	Subalkalic gabbro	Subalkalic gabbro	Subalkalic gabbro	Subalkalic gabbro
Host mineral	Amphibole	Amphibole	Amphibole	Amphibole	Amphibole	Amphibole	Amphibole	Amphibole
Inclusion-type	Cu-rich SL	Cu-rich SL	Cu-rich SL	MSS	MSS	MSS	MSS	MSS
S (wt %)	42.0	40.3	39.9	43.8	38.4	40.7	39.6	33.0
Fe (wt %)	46.6	46.8	47.9	51.5	57.3	57	55	61
Co (wt %)	0.5	0.8	0.5	0.3	0.3	0.1	0.4	0.4
Ni (wt %)	1.0	2.1	1.4	1.0	1.0	0.7	0.4	0.5
Cu (wt %)	9.6	9.7	9.8	3.1	2.7	1.6	4.8	5.0
Zn (ppm)	660.5	223.6	475.3	462.5	124.2	98.1	147.9	183.7
As (ppm)	<1.4	<13.6	<3.7	<7.6	<6.8	<10.2	<3.2	<6.0
Se (ppm)	91.3	73.1	108.7	117.8	107.6	70.9	35.7	51.1
Mo (ppm)	3	19.1	77.2	18.7	<0.4	<0.7	16.6	34.2
Ru (ppm)	<0.04	<0.5	<0.1	<0.3	<0.3	<0.8	<0.1	<0.3
Rh (ppm)	<0.01	<0.08	<0.02	<0.08	<0.05	<0.10	0.04	<0.05
Pd (ppm)	5.2	3.1	9.5	1.06	3.1	10.6	<0.2	<0.2
Ag (ppm)	44.8	11.0	34.4	5.1	<2.9	<5.1	<1.07	<2.3
Cd (ppm)	3.6	<4.1	1.7	<0.9	<0.8	<3.2	2.01	<1
In (ppm)	0.05	<0.04	<0.2	<0.2	<0.2	<0.2	<0.1	<0.2
Sn (ppm)	n.a.	n.a.	n.a.	n.a.	n.a.	n.a.	n.a.	n.a.
Sb (ppm)	n.a.	n.a.	n.a.	n.a.	n.a.	n.a.	n.a.	n.a.
Te (ppm)	n.a.	n.a.	n.a.	n.a.	n.a.	n.a.	n.a.	n.a.
Re (ppm)	0.1	<0.1	0.3	0.1	<0.1	<0.2	0.1	0.3
Os (ppm)	<0.03	<0.3	<0.09	<0.2	<0.3	<0.5	<0.1	<0.2
Ir (ppm)	0.02	<0.1	0.07	<0.1	<0.1	<0.1	<0.02	<0.08
Pt (ppm)	0.4	<0.5	0.26	<0.3	<0.8	<0.4	0.52	<0.1
Au (ppm)	0.4	1.4	1.05	0.6	0.1	<0.2	0.2	0.3
Hg (ppm)	n.a.	n.a.	n.a.	n.a.	n.a.	n.a.	n.a.	n.a.
Pb (ppm)	2.4	2.2	1.9	1.1	0.7	<0.2	<0.09	0.7
Bi (ppm)	n.a.	n.a.	n.a.	n.a.	n.a.	n.a.	n.a.	n.a.
Mg number								

Inclusions	K4-2	K4-3	K4-4	K4-5	K4-6	K4-7	K4-8	K20	LoD
Rock type	Subalkalic gabbro	Subalkalic gabbro	Subalkalic gabbro	Subalkalic gabbro	Subalkalic gabbro	Subalkalic gabbro	Subalkalic gabbro	Subalkalic gabbro	
Host mineral	Amphibole	Amphibole	Amphibole	Amphibole	Amphibole	Amphibole	Amphibole	Amphibole	
Inclusion-type	MSS	MSS	MSS	MSS	MSS	MSS	MSS	MSS	
S (wt %)	33.0	45.3	40.3	39.2	36.5	41.6	43.4	43.5	
Fe (wt %)	61	50	53.5	56.5	62	53.7	51.7	50.5	
Co (wt %)	0.4	0.3	0.3	0.3	0.3	0.5	0.3	0.2	
Ni (wt %)	0.5	0.4	0.4	0.3	0.3	0.6	0.4	1.0	
Cu (wt %)	5.0	4.4	5.9	4.2	1.1	3.7	4.3	4.5	
Zn (ppm)	183.7	–2.1	161.5	79.5	244.0	457.0	154.1	58.7	0.7–26
As (ppm)	<6.0	<1.4	<0.5	7.03	<8.8	<18.1	<2.4	<1.8	0.5–18
Se (ppm)	51.1	119.3	53.5	51.5	63.8	68.2	54.0	17.9	1.6–44
Mo (ppm)	34.2	1.13	0.94	57.8	<0.8	<1.5	<0.1	0.1	0.05–5.6
Ru (ppm)	<0.3	<0.08	<0.02	<0.05	<0.4	<0.8	<0.1	<0.09	0.03–0.9
Rh (ppm)	<0.05	<0.02	<0.005	<0.10	<0.20	<0.1	<0.1	<0.01	0.01–0.2
Pd (ppm)	<0.2	<0.1	<0.01	<0.03	<0.2	<0.4	<0.1	0.09	0.02–0.7
Ag (ppm)	<2.3	2.4	3.1	2.6	<3.9	<8.2	3.6	3	0.1–8
Cd (ppm)	<1	<0.4	0.2	<0.4	<2.7	1.3	0.4	<0.4	0.1–6
In (ppm)	<0.2	0.05	<0.01	<0.04	<0.3	<0.4	0.0	<0.02	0.02–0.4
Sn (ppm)	n.a.	n.a.	n.a.	n.a.	n.a.	n.a.	n.a.	n.a.	0.1–1
Sb (ppm)	n.a.	n.a.	n.a.	n.a.	n.a.	n.a.	n.a.	n.a.	0.08–0.6
Te (ppm)	n.a.	n.a.	n.a.	n.a.	n.a.	n.a.	n.a.	n.a.	0.7–6
Re (ppm)	0.3	<0.04	0.03	0.4	<0.1	<0.6	0.0	<0.03	0.02–0.6
Os (ppm)	<0.2	<0.05	<0.01	<0.03	<0.2	<0.5	<0.1	<0.06	0.02–0.6
Ir (ppm)	<0.08	<0.01	0.01	0.04	<0.08	<0.1	0.0	<0.01	0.01–0.1
Pt (ppm)	<0.1	<0.06	<0.02	1.2	<0.7	<1.4	<0.1	<0.07	0.02–1.4
Au (ppm)	0.3	0.7	<0.01	0.8	<0.1	0.1	0.0	<0.02	0.01–0.6
Hg (ppm)	n.a.	n.a.	n.a.	n.a.	n.a.	n.a.	n.a.	n.a.	1.5–10
Pb (ppm)	0.7	0.8	1.6	1.4	1.5	2.5	1.2	1.2	0.02–0.7
Bi (ppm)	n.a.	n.a.	n.a.	n.a.	n.a.	n.a.	n.a.	n.a.	0.02–0.1
Mg number									

Notes: n.a. = not analyzed, LoD = limit of detection, L = sulfide liquid

fide inclusions of such composition are not uncommon and have been reported from the Flatreef, Bushveld Complex, a layered igneous intrusion in South Africa (Holwell et al., 2011) and from the mafic xenoliths of the Santa Rita and Cerrillos porphyry Cu deposits, formed in an arc setting in New Mexico (Chang and Audétat, 2018).

The MSS- and Cu-rich sulfide inclusions of the Chilas Complex could represent cumulate and fractionated liquid components of an initial sulfide melt. The question of what proportion to use for each component is not evident. However, several studies propose that the average of sulfides in a deposit may approximate the composition of the unfractionated sulfide melt (e.g., Keays and Lightfoot, 2004). In addition, the composition of the calculated unfractionated sulfide melt should lie along the tie lines between the MSS field and the sulfide melt (SL, Fig. 4B). Therefore, we assume that the average of samples containing both MSS- and Cu-rich inclusions (Table 2) is a reasonable approximation for the bulk composition of the original sulfide melt. The major element composition of such a melt would be 37.2 ± 2.5 wt % S, 47.5 ± 2.7 wt % Fe, 8.6 ± 1.3 wt % Cu, 6.2 ± 0.8 wt % Ni, and 0.5 ± 0.2 wt % Co (see Table A4 for trace elements). This approach likely overestimates the amount of Cu in the sulfide melt because the Cu content of some of the K11b inclusions approaches the composition of ISS (Cu = 31.6 ± 2.7 wt %). A preferred estimate excludes ISS-like compositions from the average, and yields a primary sulfide melt with 37.7 ± 1.8 wt % S, 47 ± 1.7 wt % Fe, 6.8 ± 0.8 wt % Cu, 7 ± 0.8 wt % Ni, and 0.5 ± 0.1 wt % Co (see Table A4 for trace elements). The composition of the estimated primary sulfide melts is indicated in Figure 4B as SL I, for the estimate including ISS-like compositions, and SL II, for the estimate excluding ISS-like compositions.

Chalcophile element concentrations in the parental and derivative magmas

The chalcophile element concentration in the parental and derivative magmas (silicate melts) of the Chilas Complex were calculated based on the estimated composition of the calculated sulfide melt, using the mass balance equation for the relative mass of silicate melt that could have interacted with sulfide liquid (the R factor of Campbell and Naldrett, 1979). This requires estimates of the $D^{sulf/sil}$: 1,500 (Cu), 6,300 (Au), 2×10^5 (Pd), 8.5×10^5 (Pt), 4.2×10^5 (Ru), 2×10^5 (Rh), and 5×10^5 (Ir) (Mungall and Brenan, 2014); 800 (Ag) and 300 (Bi) (Li and Audétat, 2012); Se (D = 550) and Te (D = 6,100) (Brenan, 2015). Some of the experimental work cited includes data for various ranges in oxygen fugacity (f_{O_2}). In those cases, we used the average values from experiments conducted at $\Delta_{FMQ} \geq 0$ because of the relatively oxidized nature of arc magmas (Ballhaus et al., 1990).

The other parameter required, the R factor, can be approximated from mantle-normalized metal patterns. Barnes et al. (1993) and Barnes and Ripley (2016) have shown that elements with different partition coefficients show similar enrichment in sulfides if the R factor is less than 3,000. Enrichment of Cu (D = 1,500) and Pd ($D = 2 \times 10^5$) in sulfide melt does not diverge much if the R factor is roughly less than 3,000, resulting in mantle-normalized patterns showing no significant enrichment of Pd over Cu. The mantle-normalized diagram for our sulfide inclusion data (Fig. 4C) shows no Pd over Cu enrichment, suggesting that these inclusions formed at an R factor ≤3,000; therefore, a range of R factors (from 1,000–3,000) was assumed. The proposed R factors are consistent with the range of R factors proposed for primitive arc magmas (Richards 2009). Similar R factors have been estimated for some magmatic deposits, for example, Sudbury (R factor of 700–1,000; Mungall et. al., 2005) and for the disseminated sulfides of the Talnakh and Kharaelakh deposits (R factor of ~3,000; Barnes and Ripley, 2016). Extending the range of the R factor to a lower limit of 1,000 and an upper limit of 10,000 does not significantly change our results (Fig. 4C).

The metal concentrations in the parental silicate melt were calculated using the protocol summarized in Table A4. The model may underestimate elements compatible in silicate phases that fractionate before sulfide saturation, as it is based on element concentration in sulfide melts. Sulfide inclusions hosted in olivine with an Mg number (Mg number = (Mg/(Mg + Fe)) of ~0.84 within the dunites suggests that the crystallized silicate fraction before sulfide saturation was minor. However, Ni was not included in the model because it is compatible in olivine (Mavrogenes and O'Neill, 1999). None of the other chalcophile elements considered are expected to be significantly lost to the crystallized silicate fraction prior to sulfide saturation (Li and Audétat, 2012; Mungall and Brenan, 2014; Brenan, 2015).

The calculated parental magma compositions for the Chilas Complex rocks (Fig. 4D) show strong depletions in Pt, Rh, Ru, and Ir; minor, or no depletion in Bi, Te, Au, and Pd, and some enrichment in Se, Cu, and Ag relative to the primitive upper mantle (Fig. 4D). The model (Fig. 4D, Table A4) indicates that the parental magma was already depleted in IPGE before reaching the lower crust, likely due to the well-known compatibility of IPGE in the mantle during partial melting (e.g., Alard et al., 2000; Barnes and Lightfoot, 2005). Depleted mantle-normalized whole-rock metal patterns (Fig. 4A) and lack of detectable IPGE in MSS-type inclusions (Fig. 4C; Table 2) further supports the interpretation that IPGE were retained in mantle residue. Palladium, Au, and Cu were fully mobilized from the mantle source, as shown from their relatively high concentrations in the modeled parental melt, perhaps due to the complete mobilization of Cu-rich interstitial sulfides into partial melt (e.g., Alard et al., 2000). Our model predicts low concentrations (0.04–0.5 ppb) of Pt in the calculated parental melt compared to Pd (1.2–8 ppb) due to the lower Pt concentration (0.1–0.5 ppm) in the interpreted sulfide melt compared to Pd (3.5–8 ppm; Table A4). The relatively low concentration of Pt in sulfides suggests that other phases may control the Pt budget, in addition to sulfides. This could be attributed to early crystallization of Pt-rich alloys or Cr spinel fractionation prior to sulfide saturation (e.g., Alard et al., 2000; Park et al., 2016). However, we observe no supporting evidence for the latter, as analyzed spinel inclusions contained no detectable PGE (Fig. A1). Another possible explanation is that mantle wedge metasomatism caused by subducted slab fluids could have contributed to the relatively high Pd (1.2–8 ppb), Au (0.2–1.5 ppb), and Cu (70–140 ppm) concentrations of the calculated melt (e.g., Noll, Jr. et al., 1996; Rielli et al., 2018). Our estimates are consistent with the concentrations of chalcophile elements observed in picrites

from Granada, Lesser Antilles arc (Woodland et al., 2002) and the Pual Ridge arc lavas, eastern Manus Basin (Park et al., 2013; Fig. 4D). They are also consistenet with the Cu contents (50–90 ppm) of primitive arc magmas (Lee et al., 2012) and low degrees of sulfide saturation at the Tolbachik volcano, Kamchatka (Zelenski et al., 2018).

From mass balance calculations, the mass fraction of sulfides segregated by the Chilas Complex lower crust was calculated using equation 3 in Barnes et al. (1993):

$$C_d/C_i=[1 + X (D – 1)/100],$$

where, C_d = concentration of an element in the derivative/fractionated melt, and was calculated from sulfide/silicate melt partition coefficient, C_i = concentration of an element in the parental melt, X = wt % sulfides, and D = partition coefficient.

The mass fraction of segregated sulfides ranges from 0.1 to 0.17 wt % which is consistent with the sulfide fraction (~0.1–0.2 wt %) calculated for other sulfide saturated magmas (e.g., Lightfoot and Keays, 2005; Jamais et al., 2008; Cocker et al., 2016; Hao et al., 2019). The percentage of metal lost due to the segregation of sulfides was then calculated by dividing the element concentration in the derivative silicate melt (C_d) by parental melt (C_i), the depletion factor. The calculated results (Fig. 5) show that the segregated sulfides would deplete the residual melt by >95% of its Pd, Pt, Rh, Ru, and Ir, 33 to 86% of its Au, 13 to 60% of Cu, 7 to 44% of Ag, 5 to 35% of Se, and 3 to 23% of Bi. Copper in the derivative melt (Figs. 4D, 5) is less affected by the segregation of sulfides than Au and PGE because of its relatively lower partition coefficient in sulfide melt, relatively greater abundance in the parental silicate melt, and the small volumes of fractionating sulfide in the lower crust.

Implications for arc metallogeny

Our results support models of arc metallogeny in which subduction-related magmas, produced by partial melting of a metasomatized mantle wedge, are depleted in PGE ± Au by sulfide segregation in the lower crust. However, the magmas transport sufficient concentration of Cu (Fig. 4D; Table A4) into the upper crust to generate the most common type of porphyry deposits, which are Cu-rich but PGE-poor (e.g., Richards, 2011; Cocker et al., 2016; Du and Audétat, 2020). In contrast, we did not find evidence for relatively voluminous (~1%) precipitation of sulfides in the Chilas Complex magmas, as suggested by the models of Lee et al. (2012), Chen et al. (2020), and Lee and Tang (2020). Therefore, a second stage of melting of lower crust cumulates may not be required to generate Cu-rich magmas as precursors for normal arc-related porphyry Cu deposits.

However, there are no known porphyry deposits in the upper section of the Kohistan arc, suggesting that porphyry deposits are formed from the optimized combination of multiple processes operating at lower and upper crustal levels. Elimination of any of these processes may result in the failure of a deposit to form (e.g., Richards, 2005). Also, our results provide constraints to evaluate the influence of sulfide saturation only in the Chilas Complex lower crust, and variations across arc settings are possible. Therefore, further studies on other lower crustal arc sections, such as the Talkeetna arc in Alaska (Greene et al., 2006) and the Sierra Valle Fertil arc in Argentina (Walker et al., 2015) are required to understand if the same processes operate globally.

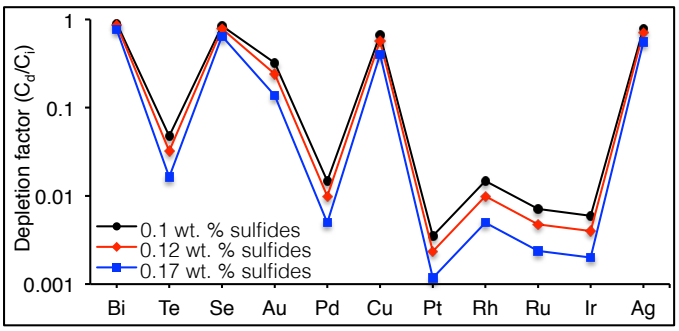

Fig. 5. Calculated depletion factors (C_d/C_i) of selected chalcophile elements, where C_d is the concentration of the element in fractionated magma after segregation of sulfides and C_i is the concentration of the element in the parental magma.

Conclusions

The ultramafic-mafic lower crust of the Kohistan arc contains a small amount of residual magmatic sulfides (0.1–0.17 wt %), with sulfides containing up to 34 wt % Cu, 23 ppm Au, 245 ppm Pd, and 20 ppm Pt. Mass balance calculations indicate that the parental magmas from which these rocks crystallized were depleted in IPGE but not in Cu, Au, and Pd before entering the lower crust. Segregation of a small amount (<0.2 wt %) of sulfide liquid from the parental magma depleted the derivative magma in PGE and Au because of their very high $D^{sulf/sil}$. The PGE-depleted magma that ascended from these lower crustal cumulate zones retained sufficient Cu to potentially form porphyry Cu but PGE-depleted deposits in the shallow crust, as commonly observed in arc settings.

Acknowledgments

This work comprises part of IA's Ph.D. research and was supported by a Discovery Grant from the Natural Sciences and Engineering Research Council of Canada to JPR (RGPIN203099) and a Canada Excellence Research Chair grant to DGP. IA acknowledges financial support from the Harquail School of Earth Sciences, a student Research Grant from the Society of Economic Geologists for additional analyses, and the University of Peshawar for fieldwork support. Garrett Harris and Janina Czas helped with whole-rock HSE analyses, Martin von Dollen with polished thin sections, and Andrew Locock with electron probe microanalyses. We thank Ali Sholeh for the editorial handling of the paper, and Jeffrey Hedenquist, Adam C. Simon, Keiko Hattori, and an anonymous reviewer for their reviews.

REFERENCES

Alard, O., Griffin, W.L., Lorand, J.P., Jackson, S.E., and O'Reilly, S.Y., 2000, Non-chondritic distribution of the highly siderophile elements in mantle sulphides: Nature, v. 407, p. 891–894.

Ballhaus, C., Berry, R., and Green, D., 1990, Oxygen fugacity controls in the Earth's upper mantle: Nature, v. 348, p. 437–440.

Barnes, S.-J., and Lightfoot, P.C., 2005, Formation of magmatic nickel-sulfide ore deposits and processses affecting their copper and platinum-group element contents: Economic Geology 100th Anniversary, p. 179–213.

Barnes, S.-J., and Ripley, E.M., 2016, Highly siderophile and strongly

chalcophile elements in magmatic ore deposits: Reviews in Mineralogy and Geochemistry, v. 81, p. 725–774.
Barnes, S.-J., Couture, J.-F., Sawyer, E.W., and Bouchaib, C., 1993, Nickel-copper occurrences in the Belleterre-Angliers belt of the Pontiac Subprovince and the use of Cu-Pd ratios in interpreting platinum-group element distributions: Economic Geology, v. 88, p. 1402–1418.
Becker, H., Horan, M.F., Walker, R.J., Gao, S., Lorand, J.P., and Rudnick, R.L., 2006, Highly siderophile element composition of the Earth's primitive upper mantle: Constraints from new data on peridotite massifs and xenoliths: Geochimica et Cosmochimica Acta, v. 70, p. 4528–4550.
Bouilhol, P., Jagoutz, O., Hanchar, J.M., and Dudas, F.O., 2013, Dating the India-Eurasia collision through arc magmatic records: Earth and Planetary Science Letters, v. 366, p. 163–175.
Brenan, J.M., 2015, Se-Te fractionation by sulfide-silicate melt partitioning: Implications for the composition of mantle-derived magmas and their melting residues: Earth and Planetary Science Letters, v. 422, p. 45–57.
Burg, J.-P., 2011, The Asia-Kohistan-India collision: Review and discussion: Arc-continent collision: New York, Springer, p. 279–309.
Burg, J.-P., Jagoutz, O., Dawood, H., and Hussain, S.S., 2006, Precollision tilt of crustal blocks in rifted island arcs: Structural evidence from the Kohistan arc: Tectonics, v. 25, p. 1–13.
Cabri, L.J., 1973, New data on phase relations in the Cu-Fe-S system: Economic Geology, v. 68, p. 443–454.
Campbell, I.H., and Naldrett, A.J., 1979, The influence of silicate:sulfide ratios on the geochemistry of magmatic sulfides: Economic Geology, v. 74, p. 1503–1506.
Carroll, M.R., and Rutherford, M.J., 1985, Sulfide and sulfate saturation in hydrous silicate melts: Journal of Geophysical Research, v. 90, Supp., p. C601–C612.
Chang, J., and Audétat, A., 2018, Petrogenesis and metal content of hornblende-rich xenoliths from two Laramide-age magma systems in southwestern USA: Insights into the metal budget of arc magmas: Journal of Petrology, v. 59, p. 1869–1898.
Chen, K., Tang, M., Lee, C.-T.A., Wang, Z., Zou, Z., Hu, Z., and Liu, Y., 2020, Sulfide-bearing cumulates in deep continental arcs: The missing copper reservoir: Earth and Planetary Science Letters, v. 531, p. 115971.
Chiaradia, M., 2014, Copper enrichment in arc magmas controlled by overriding plate thickness: Nature Geoscience, v. 7, p. 43–46.
Cocker, H.A., Valente, D.L., Park, J.-W., and Campbell, I.H., 2016, Using platinum group elements to identify sulfide saturation in a porphyry Cu system: the El Abra porphyry Cu deposit, northern Chile: Journal of Petrology, v. 56, p. 2491–2514.
De Hoog, J., Hattori, K., and Hoblitt, R., 2003, Oxidized sulfur-rich mafic magma at Mount Pinatubo, Philippines: Contributions to Mineralogy and Petrology, v. 146, p. 750–761.
Du, J.A., and Audétat, A., 2020, Early sulfide saturation is not detrimental to porphyry Cu-Au formation: Geology, v. 48, p. 519–524.
Evans, K.A., and Tomkins, A.G., 2011, The relationship between subduction zone redox budget and arc magma fertility: Earth and Planetary Science Letters, v. 308, p. 401–409.
Fiorentini, M.L., Bekker, A., Rouxel, O., Wing, B.A., Maier, W., and Rumble, D., 2012, Multiple sulfur and iron isotope composition of magmatic Ni-Cu-(PGE) sulfide mineralization from eastern Botswana: Economic Geology, v. 107, p. 105–116.
Gannoun, A., Burton, K.W., Day, J.M.D., Harvey, J., Schiano, P., and Parkinson, I., 2016, Highly siderophile element and Os isotope systematics of volcanic rocks at divergent and convergent plate boundaries and in intraplate settings: Reviews in Mineralogy and Geochemistry, v. 81, p. 651–724.
Greene, A.R., DeBari, S.M., Kelemen, P.B., Blusztajn, J., and Clift, P.D., 2006, A detailed geochemical study of island arc crust: the Talkeetna arc section, south-central Alaska: Journal of Petrology, v. 47, p. 1051–1093.
Grinenko, L., 1985, Sources of sulfur of the nickeliferous and barren gabbro-dolerite intrusions of the northwest Siberian platform: International Geology Review, v. 27, p. 695–708.
Hao, H., Campbell, I.H., Richards, J.P., Nakamura, E., and Sakaguchi, C., 2019, Platinum-group element geochemistry of the Escondida igneous suites, northern Chile: Implications for ore formation: Journal of Petrology, v. 60, p. 487–514.
Holwell, D.A., and McDonald, I., 2010, A review of the behaviour of platinum group elements within natural magmatic sulfide ore systems: Platinum Metals Review, v. 54, p. 26–36.
Holwell, D.A., McDonald, I., and Butler, I.B., 2011, Precious metal enrichment in the Platreef, Bushveld Complex, South Africa: Evidence from homogenized magmatic sulfide melt inclusions: Contributions to Mineralogy and Petrology, v. 161, p. 1011–1026.
Holwell, D.A., Fiorentini, M., McDonald, I., Lu, Y., Giuliani, A., Smith, D.J., Keith, M., and Locmelis, M., 2019, A metasomatized lithospheric mantle control on the metallogenic signature of post-subduction magmatism: Nature Communications, v. 10, p. 3511.
Jagoutz, O., Muntener, O., Burg, J., Ulmer, P., and Jagoutz, E., 2006, Lower continental crust formation through focused flow in km-scale melt conduits: The zoned ultramafic bodies of the Chilas Complex in the Kohistan island arc (NW Pakistan): Earth and Planetary Science Letters, v. 242, p. 320–342.
Jagoutz, O.E., Burg, J.P., Hussain, S., Dawood, H., Pettke, T., Iizuka, T., and Maruyama, S., 2009, Construction of the granitoid crust of an island arc. Part I: Geochronological and geochemical constraints from the plutonic Kohistan (NW Pakistan): Contributions to Mineralogy and Petrology, v. 158, p. 739–755.
Jagoutz, O., Royden, L., Holt, A.F., and Becker, T.W., 2015, Anomalously fast convergence of India and Eurasia caused by double subduction: Nature Geoscience, v. 8, p. 475–478.
Jamais, M., Lassiter, J., and Brügmann, G., 2008, PGE and Os-isotopic variations in lavas from Kohala Volcano, Hawaii: Constraints on PGE behavior and melt/crust interaction: Chemical Geology, v. 250, p. 16–28.
Jenner, F.E., 2017, Cumulate causes for the low contents of sulfide-loving elements in the continental crust: Nature Geoscience, v. 10, p. 524–529.
Jenner, F.E., O'Neill, H.S.C., Arculus, R.J., and Mavrogenes, J.A., 2010, The magnetite crisis in the evolution of arc-related magmas and the initial concentration of Au, Ag and Cu: Journal of Petrology, v. 51, p. 2445–2464.
Jochum, K.P., Nohl, U., Herwig, K., Lammel, E., Stoll, B., and Hofmann, A.W., 2005, GeoReM: A new geochemical database for reference materials and isotopic standards: Geostandards and Geoanalytical Research, v. 29, p. 333–338.
Jugo, P.J., 2009, Sulfur content at sulfide saturation in oxidized magmas: Geology, v. 37, p. 415–418.
Jugo, P.J., Wilke, M., and Botcharnikov, R.E., 2010, Sulfur K-edge XANES analysis of natural and synthetic basaltic glasses: Implications for S speciation and S content as function of oxygen fugacity: Geochimica et Cosmochimica Acta, v. 74, p. 5926–5938.
Keays, R.R., and Lightfoot, P.C., 2004, Formation of Ni-Cu-platinum group element sulfide mineralization in the Sudbury impact melt sheet: Mineralogy and Petrology, v. 82, p. 217–258.
——2010, Crustal sulfur is required to form magmatic Ni-Cu sulfide deposits: Evidence from chalcophile element signatures of Siberian and Deccan Trap basalts: Mineralium Deposita, v. 45, p. 241–257.
Khan, M.A., Jan, M.Q., Windley, B.F., Tarney, J., and Thirlwall, M.F., 1989, The Chilas mafic-ultramafic igneous complex: the root of the Kohistan island arc in the Himalaya of northern Pakistan: Geological Society of America Special Paper 232, p. 75–94.
Khan, M.A., Jan, M.Q., and Weaver, B., 1993, Evolution of the lower arc crust in Kohistan, N. Pakistan: Temporal arc magmatism through early, mature and intra-arc rift stages: Geological Society, London, Special Publication 74, p. 123–138.
Khan, S.D., Walker, D.J., Hall, S.A., Burke, K.C., Shah, M.T., and Stockli, L., 2009, Did the Kohistan-Ladakh island arc collide first with India?: Geological Society of America Bulletin, v. 121, p. 366–384.
Kosyakov, V., and Sinyakova, E., 2012, Physicochemical prerequisites for the formation of primary orebody zoning at copper-nickel sulfide deposits (by the example of the systems Fe-Ni-S and Cu-Fe-S): Russian Geology and Geophysics, v. 53, p. 861–882.
Kullerud, G., Yund, R.A., and Moh, G.H., 1969, Phase relations in the Cu-Fe-S, Cu-Ni-S and Fe-Ni-S system: Economic Geology Monograph 4, p. 323–343.
Lee, C.-T.A., and Tang, M., 2020, How to make porphyry copper deposits: Earth and Planetary Science Letters, v. 529, p. 115868.
Lee, C.-T., Leeman, W.P., Canil, D., and Li, Z.-X.A., 2005, Similar V/Sc systematics in MORB and arc basalts: Implications for the oxygen fugacities of their mantle source regions: Journal of Petrology, v. 46, p. 2313–2336.
Lee, C.-T.A., Luffi, P., Le Roux, V., Dasgupta, R., Albaréde, F., and Leeman, W.P., 2010, The redox state of arc mantle using Zn/Fe systematics: Nature, v. 468, no. 7324, p. 681.
Lee, C.-T.A., Luffi, P., Chin, E.J., Bouchet, R., Dasgupta, R., Morton, D.M., Le Roux, V., Yin, Q.-z., and Jin, D., 2012, Copper systematics in arc magmas and implications for crust-mantle differentiation: Science, v. 336, p. 64–68.
Lesher, C.M., and Burnham, O.M., 2001, Multicomponent elemental and

isotopic mixing in Ni-Cu-(PGE) ores at Kambalda, Western Australia: Canadian Mineralogist, v. 39, p. 421–446.
Li, Y., and Audétat, A., 2012, Partitioning of V, Mn, Co, Ni, Cu, Zn, As, Mo, Ag, Sn, Sb, W, Au, Pb, and Bi between sulfide phases and hydrous basanite melt at upper mantle conditions: Earth and Planetary Science Letters, v. 355–356, p. 327–340.
Lightfoot, P.C., and Keays, R.R., 2005, Siderophile and chalcophile metal variations in flood basalts from the Siberian trap, Noril'sk region: Implications for the origin of the Ni-Cu-PGE sulfide ores: Economic Geology, v. 100, p. 439–462.
Liu, J., and Pearson, D.G., 2014, Rapid, precise and accurate Os isotope ratio measurements of nanogram to sub-nanogram amounts using multiple Faraday collectors and amplifiers equipped with 1012 Ω resistors by N-TIMS: Chemical Geology, v. 363, p. 301–311.
Liu, Y., and Brenan, J., 2015, Partitioning of platinum-group elements (PGE) and chalcogens (Se, Te, As, Sb, Bi) between monosulfide-solid solution (MSS), intermediate solid solution (ISS) and sulfide liquid at controlled f_{O_2}-f_{S_2} conditions: Geochimica et Cosmochimica Acta, v. 159, p. 139–161.
Mallmann, G., and O'Neill, H.S.C., 2009, The crystal/melt partitioning of v during mantle melting as a function of oxygen fugacity compared with some other elements (Al, P, Ca, Sc, Ti, Cr, Fe, Ga, Y, Zr and Nb): Journal of Petrology, v. 50, p. 1765–1794.
Mansur, E.T., Barnes, S.-J., and Duran, C.J., 2020, An overview of chalcophile element contents of pyrrhotite, pentlandite, chalcopyrite, and pyrite from magmatic Ni-Cu-PGE sulfide deposits: Mineralium Deposita, v. 56, p. 1–26.
Mavrogenes, J.A., and O'Neill, H.S.C., 1999, The relative effects of pressure, temperature and oxygen fugacity on the solubility of sulfide in mafic magmas: Geochimica et Cosmochimica Acta, v. 63, p. 1173–1180.
Mikoshiba, M.U., Takahashi, Y., Takahashi, Y., Kausar, A.B., Khan, T., Kubo, K., and Shirahase, T., 1999, Rb-Sr isotopic study of the Chilas Igneous Complex, Kohistan, northern Pakistan: Geological Society of America Special Paper 328, p. 47–57.
Mungall, J.E., and Brenan, J.M., 2014, Partitioning of platinum-group elements and Au between sulfide liquid and basalt and the origins of mantle-crust fractionation of the chalcophile elements: Geochimica et Cosmochimica Acta, v. 125, p. 265–289.
Mungall, J.E., Andrews, D.R.A., Cabri, L.J., Sylvester, P.J., and Tubrett, M., 2005, Partitioning of Cu, Ni, Au, and platinum-group elements between monosulfide solid solution and sulfide melt under controlled oxygen and sulfur fugacities: Geochimica et Cosmochimica Acta, v. 69, p. 4349–4360.
Noll, P., Jr., Newsom, H., Leeman, W., and Ryan, J.G., 1996, The role of hydrothermal fluids in the production of subduction zone magmas: Evidence from siderophile and chalcophile trace elements and boron: Geochimica et Cosmochimica Acta, v. 60, p. 587–611.
Palme, H., and O'Neill, H.S.C., 2014, Cosmochemical estimates of mantle composition: Treatise on Geochemistry, v. 2, p. 1–39.
Park, J.-W., Campbell, I.H., and Arculus, R.J., 2013, Platinum-alloy and sulfur saturation in an arc-related basalt to rhyolite suite: Evidence from the Pual Ridge lavas, the eastern Manus Basin: Geochimica et Cosmochimica Acta, v. 101, p. 76–95.
Park, J.-W., Campbell, I.H., and Kim, J., 2016, Abundances of platinum group elements in native sulfur condensates from the Niuatahi-Motutahi submarine volcano, Tonga rear arc: Implications for PGE mineralization in porphyry deposits: Geochimica et Cosmochimica Acta, v. 174, p. 236–246.
Patriat, P., and Achache, J., 1984, India-Eurasia collision chronology has implications for crustal shortening and driving mechanism of plates: Nature, v. 311, p. 615–621.
Patten, C., Barnes, S.J., Mathez, E.A., and Jenner, F.E., 2013, Partition coefficients of chalcophile elements between sulfide and silicate melts and the early crystallization history of sulfide liquid: LA-ICP-MS analysis of MORB sulfide droplets: Chemical Geology, v. 358, p. 170–188.
Pearson, D.G., and Woodland, S.J., 2000, Solvent extraction/anion exchange separation and determination of PGEs (Os, Ir, Pt, Pd, Ru) and Re-Os isotopes in geological samples by isotope dilution ICP-MS: Chemical Geology, v. 165, p. 87–107.
Pearson, D.G., Parman, S.W., and Nowell, G.M., 2007, A link between large mantle melting events and continent growth seen in osmium isotopes: Nature, v. 449, p. 202–205.
Petterson, M.G., 2010, A review of the geology and tectonics of the Kohistan island arc, north Pakistan: Geological Society, London, Special Publication 338, p. 287–327.
——2019, The plutonic crust of Kohistan and volcanic crust of Kohistan-Ladakh, north Pakistan/India: Lessons learned for deep and shallow arc processes: Geological Society, London, Special Publication 483, p. 123–164.
Petterson, M.G., and Treloar, P.J., 2004, Volcanostratigraphy of arc volcanic sequences in the Kohistan arc, north Pakistan: Volcanism within island arc, back-arc-basin, and intra-continental tectonic settings: Journal of Volcanology and Geothermal Research, v. 130, p. 147–178.
Petterson, M.G., and Windley, B.F., 1985, Rb-Sr dating of the Kohistan arc-batholith in the Trans-Himalaya of north Pakistan, and tectonic implications: Earth and Planetary Science Letters, v. 74, p. 45–57.
Plank, T., Kelley, K.A., Zimmer, M.M., Hauri, E.H., and Wallace, P.J., 2013, Why do mafic arc magmas contain ~4 wt % water on average?: Earth and Planetary Science Letters, v. 364, p. 168–179.
Richards, J.P., 2003, Tectono-magmatic precursors for porphyry Cu-(Mo-Au) deposit formation: Economic Geology, v. 98, p. 1515–1533.
——2005, Cumulative factors in the generation of giant calc-alkaline porphyry Cu deposits: Super porphyry copper and gold deposits: A global perspective: Adelaide, PGC Publishing, v. 1, p. 7–25.
——2009, Postsubduction porphyry Cu-Au and epithermal Au deposits: Products of remelting of subduction-modified lithosphere: Geology, v. 37, p. 247–250.
——2011, Magmatic to hydrothermal metal fluxes in convergent and collided margins: Ore Geology Reviews, v. 40, p. 1–26.
Rielli, A., Tomkins, A.G., Nebel, O., Raveggi, M., Jeon, H., Martin, L., and Ávila, J.N., 2018, Sulfur isotope and PGE systematics of metasomatised mantle wedge: Earth and Planetary Science Letters, v. 497, p. 181–192.
Ripley, E.M., and Li, C., 2003, Sulfur isotope exchange and metal enrichment in the formation of magmatic Cu-Ni-(PGE) deposits: Economic Geology, v. 98, p. 635–641.
Robertson, A.H., and Collins, A.S., 2002, Shyok suture zone, N. Pakistan: Late Mesozoic-Tertiary evolution of a critical suture separating the oceanic Ladakh arc from the Asian continental margin: Journal of Asian Earth Sciences, v. 20, p. 309–351.
Robertson, J., Ripley, E.M., Barnes, S.J., and Li, C., 2015, Sulfur liberation from country rocks and incorporation in mafic magmas: Economic Geology, v. 110, p. 1111–1123.
Schaltegger, U., Zeilinger, G., Frank, M., and Burg, J.-P., 2002, Multiple mantle sources during island arc magmatism: U-Pb and Hf isotopic evidence from the Kohistan arc complex, Pakistan: Terra Nova, v. 14, p. 461–468.
Sharma, K., Blake, S., Self, S., and Krueger, A.J., 2004, SO_2 emissions from basaltic eruptions, and the excess sulfur issue: Geophysical Research Letters, v. 31, no. 13, p. 1–4.
Tahirkheli, R.A.K., and Jan, M.Q., 1979, Geology of Kohistan, Karakoram Himalaya, northern Pakistan: Journal of Himalayan Earth Sciences, v. 11, p. 1–3.
Tang, M., Erdman, M., Eldridge, G., and Lee, C.-T.A., 2018, The redox "filter" beneath magmatic orogens and the formation of continental crust: Science Advances, v. 4, no. 5, p. 1–7.
Thakurta, J., Ripley, E.M., and Li, C., 2014, Platinum group element geochemistry of sulfide-rich horizons in the Ural-Alaskan-type ultramafic complex of Duke Island, southeastern Alaska: Economic Geology, v. 109, p. 643–659.
Treloar, P.J., Petterson, M.G., Jan, M.Q., and Sullivan, M.A., 1996, A re-evaluation of the stratigraphy and evolution of the Kohistan arc sequence, Pakistan Himalaya: Implications for magmatic and tectonic arc-building processes: Journal of the Geological Society, v. 153, p. 681–693.
Van Hoose, A.E., Streck, M.J., Pallister, J.S., and Wälle, M., 2013, Sulfur evolution of the 1991 Pinatubo magmas based on apatite: Journal of Volcanology and Geothermal Research, v. 257, p. 72–89.
Walker, B.A., Bergantz, G.W., Otamendi, J.E., Ducea, M.N., and Cristofolini, E.A., 2015, A MASH zone revealed: the mafic complex of the Sierra Valle Fértil: Journal of Petrology, v. 56, p. 1863–1896.
Wallace, P.J., 2005, Volatiles in subduction zone magmas: Concentrations and fluxes based on melt inclusion and volcanic gas data: Journal of Volcanology and Geothermal Research, v. 140, p. 217–240.
Woodland, S.J., Pearson, D.G., and Thirlwall, M.F., 2002, A platinum group element and Re-Os isotope investigation of siderophile element recycling in subduction zones: Comparison of Grenada, Lesser Antilles arc, and the Izu-Bonin arc: Journal of Petrology, v. 43, p. 171–198.
Zelenski, M., Kamenetsky, V.S., Mavrogenes, J.A., Gurenko, A.A., and Danyushevsky, L.V., 2018, Silicate-sulfide liquid immiscibility in modern arc basalt (Tolbachik volcano, Kamchatka): Part I. Occurrence and compositions of sulfide melts: Chemical Geology, v. 478, p. 102–111.

Zhang, D., and Audétat, A., 2017, What caused the formation of the giant Bingham Canyon porphyry Cu-Mo-Au deposit? Insights from melt inclusions and magmatic sulfides, Economic Geology, v. 112, p. 221–244.

Zimmer, M.M., Plank, T., Hauri, E.H., Yogodzinski, G.M., Stelling, P., Larsen, J., Singer, B., Jicha, B., Mandeville, C., and Nye, C.J., 2010, The role of water in generating the calc-alkaline trend: new volatile data for Aleutian magmas and a new tholeiitic index: Journal of Petrology, v. 51, p. 2411–2444.

Ijaz Ahmad is a Ph.D. candidate at the Mineral Exploration Research Centre, Harquail School of Earth Sciences, Laurentian University, Canada. His current research focuses on the chalcophile metal budget of arc magmas and its implication on the formation of porphyry-epithermal deposits. Mr. Ahmad holds bachelor of science and master's degrees from Pakistan, followed by six years work on the RekoDiq porphyry-Cu-Au deposit, a joint venture project of Barrick Gold and Antofagasta PLC in Pakistan. He moved to Canada to pursue a master's in economic geology from the University of Alberta and later to the Laurentian University for doctoral studies.